Eur. Phys. J. B (2016) 89: 44
DOI: 10.1140/epjb/e2016-60909-9

THE EUROPEAN PHYSICAL JOURNAL B

Regular Article

Metal-ferroelectric-metal current-voltage characteristics: A charge flow balance through interfaces approach

Lucian Dragos Filip[a] and Lucian Pintilie

National Institute of Materials Physics, Atomistilor str., nr. 105bis, P.O. Box MG7, 077125 Magurele, Romania

Received 24 November 2015 / Received in final form 11 January 2016
Published online 15 February 2016 –

Abstract. A model for current voltage characteristics of a thin film metal-ferroelectric-metal structure is constructed by combining the electrostatics of a polarized ferroelectric film with the balanced flow of charge through its interfaces. Using a set of fitting parameters, good agreement with several sets of experimental data is obtained for different system temperatures. The influence of model parameters on the current-voltage characteristic is discussed. Best fit values of some of these parameters correlate well with ab initio calculations in the literature, supporting the idea of low dielectric permittivity of the interface transition layers in the ferroelectric.

1 Introduction

Thin film metal-ferroelectric-metal (MFM) heterostructures have exhibited impressive switching properties that can be directly harnessed into applications such as ferroelectric random access memories (RAM) [1–9]. One of the most important parameters to be controlled in these cases is the leakage current. In order to be used as a RAM module, the MFM device should be able to retain a ferroelectric state over extended periods of time and thus it should be a very good capacitor. Leakage currents are phenomena taking place at both interfaces of the MFM device where carriers will "leak" into electrodes, potentially destroying a prepared ferroelectric state. It is thus important to study such devices under several conditions and many research groups have characterized MFM capacitors for various temperature ranges, different metallic electrodes, ferroelectric materials, etc. [4–6,10–13]. Not surprisingly, the main conclusion of most of these studies reported the interface phenomena to be responsible for the leakage current [10,11,14–17] and since these are thin film devices, the leakage will likely be affected by the entire electrode-ferroelectric-electrode system.

Many theoretical treatments, use the general metal/semiconductor (M/S) interface theory as a starting point [18], and include the ferroelectric properties using an approximation that will be addressed below. The rather obvious downside of this model is that it will only calculate the electron current at *one of the two interfaces of the MFM device* and, while this is an acceptable approximation when a thick semiconductor is involved, the case of a thin film is not well represented. Another limitation of the current models is in the choice of the transmission mechanisms used to calculate the leakage current. Schottky emission is usually the preferred one, while electron tunnelling is more often neglected. The main reason for not including a tunnelling mechanism for all temperatures is also related to the general M/S interface theory where barrier heights are low enough for thermionic emission while the potential barrier thickness is often too large for electron tunnelling. In the case of ferroelectrics, however, the metal-ferroelectric interface is considerably more complex due to the spontaneous polarization. The most common approximation that is used to include the ferroelectric polarization is to consider its effects from the perspective of some equivalent charged sheets placed in the vicinity of each interface [2,12,19–23]. The absolute value of the charge density on each sheet is equal to the polarization value, P. Such an approximation is quite abrupt but it captures the profound effect of reducing the potential barrier thickness that the ferroelectric polarization has on the two interfaces. Equally important is the fact that the electrostatic asymmetry introduced by the polarization creates, near one of the interfaces, a high potential energy barrier that is hard to be overcome by carriers through Schottky emission only.

In this paper we propose a model for the thin film MFM structure where the electron tunnelling is considered as an important transport mechanism in the leakage current. Also it will be shown that by using a general balance equation for the incoming and outgoing currents through the structure, contributions from both interfaces can be accounted for in our formulation. Using this approach it is possible to calculate the leakage current as a function of a set of intrinsic model parameters whose values can be adjusted by comparison with measured experimental data thus providing valuable physical insight into the behaviour

[a] e-mail: lucian.filip@infim.ro

of the system. This model is by no means complete and there are many avenues where it can be improved, such as considering a continuous distribution of the polarization charge in the ferroelectric instead of the abrupt charged sheets. However, its present form can be used as a first building block for a more general theoretical description of the leakage currents in thin film MFM devices. It is in these authors opinion that only by including the entire device structure, true optimization can be performed for real life applications. The present paper is structured as follows: the theoretical model will be described together with the approximations and the reasons behind each one, followed by a discussion of the influence of model parameters on simulation results. The theoretical model will then be used to fit experimental current-voltage (I-V) characteristics obtained from three MFM samples (each with a different top electrode material) for several system temperatures and lastly conclusions and closing remarks will follow.

2 Theoretical model

The focus of the present paper is to address the complexity of the leakage current problem in a reasonably accessible description. To this purpose, several simplifying assumptions have to be made. Thus, a thin film MFM device will be considered, consisting of a ferroelectric material of thickness d sandwiched between two electrodes taken as perfect electron reservoirs able to accommodate any incoming and outgoing electron currents. The ferroelectric material will be regarded as an epitaxial thin film such that all possible issues relating to ferroelectric domains and structure defects can be safely ignored. Moreover, the ferroelectric will be considered as a homogeneous wide band gap *n-type* semiconductor [3,8], with a uniform donor density N_d. The saturated ferroelectric polarization will be described through an abrupt approximation: it is assumed as uniform in the bulk region of the film and vanishingly small in two thin layers of nanometre size where the atomic structure changes from that of a ferroelectric to the electrode materials. Being uniform, the polarization P may be equivalently assumed as generated by two oppositely charged sheets, with uniform surface densities $-P$ and $+P$ placed at the extremities of the bulk ferroelectric film [2,12,19–23]. The properties of the two peripheral regions (sometimes called "dead layers"), or indeed their existence, is still debated in the literature [13,24–29]. However, it is widely accepted [15,16,22,25,27,29–31] that polarization has a strong influence on each interface region and without trying to elucidate the actual mechanism of transitioning from a material with a certain polarization state to a metal electrode, we will further refer to the region between the point where the ferroelectric polarization is zero to the charged sheet in the ferroelectric as a transition layer (TL), with a thickness d_i (as will be further explained, the index i will take specific values for each interface). The relative dielectric permittivity in these two TLs, ε_d^i, is expected to be considerably different than that in the bulk region, ε [13,24–29]. Extensive calculations using the density functional theory framework performed by Stengel and Spaldin [24] suggest that the dielectric permittivity in these TLs is much lower than the bulk value. Lastly, the TLs will be considered as fully depleted regions.

The fact that the film is polarized certainly induces important peculiarities of the potential energy profile across it. To account for such features in a convenient manner, the structure will be divided in several regions. The Poisson equation will be solved in each of them and the proper boundary and continuity conditions will be imposed. The potential energy profile will obviously disturb the spatial distribution of the quasi-free charge carriers. Thus, deeper inside the bulk region, next to each charged sheet, two regions with perturbed charge densities will form in order to counteract the effects of polarization. These two regions will be referred to as influence layers (ILs). These should not be confused with the depletion layers that normally appear at an M/S, interface which are regions with positive charge densities, influenced by the dopant density in the semiconductor. In our case the two ILs are different from each other, in the sense that, in the vicinity of the positively charged sheet there should be an accumulation of electrons while at the negatively charged sheet the region should be depleted. The apparition of these regions is strictly connected to the presence of the two charged sheets and thus they are assumed as essentially dependent on the ferroelectric polarization and on its distribution in the ferroelectric bulk. The widths of the two ILs, w_i, are therefore considered unknown parameters which will be estimated through fitting theoretical I-V characteristics onto some experimentally obtained data. This approach is clearly helpful in dealing with the problem in a simplified, non-recursive manner in which there is not enough information to solve the Poisson equation in each such region.

In the remaining bulk area, between the two ILs, the electric field is considered to be completely screened by the high doping [30–32]. This may seem like a strong approximation and, in the context of a thin film device, it probably is. However one must not forget that the bulk dielectric permitivity is usually quite large (ranging between 80 and 300 or even higher [12,14]) which suggests a high density of mobile charges that could be responsible for the electric field screening. Such an approach is not uncommon in the literature and it allows one to concentrate on the interface phenomena which appear to be the most influential on the leakage-current [27,31,32]. Figure 1, while not drawn to scale, shows a visual representation of all the regions described above.

Before any calculation of the leakage current is performed, one needs to obtain the potential energy profile for the entire structure using the indicated definitions and approximations (this should actually be the case for any related model: approximations are included at this level and not in the final result!). Prior to solving the Poisson equation in every region we need to clarify the naming of various parameters. First of all, the two electrodes will be referred to as t (top) and b (bottom) and each one,

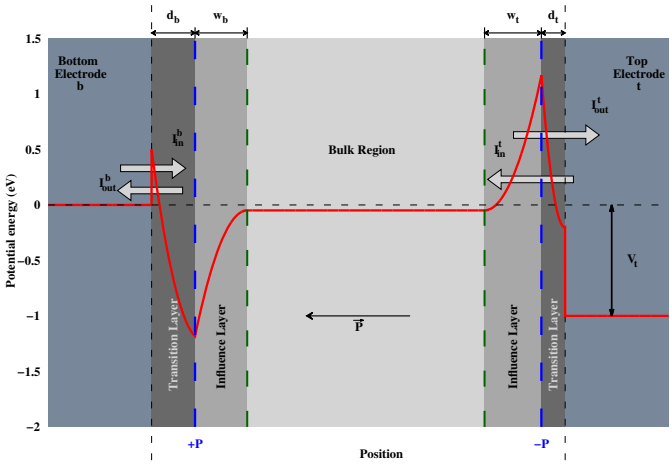

Fig. 1. Sketch of the MFM capacitor. The TLs are marked with a dark shade of grey while the ILs are shown with a slightly lighter shade. The thick red line represents the calculated potential energy. Also marked with arrows are the incoming and outgoing currents through each interface. Figure is not drawn to scale!

in turn, will play the role of the anode. This notation is intended to be consistent with the way such devices are manufactured: the epitaxial ferroelectric layer is grown on the bottom electrode and the top electrode is deposited in the final stage. The measurements are then performed by using each of the electrodes as the anode after the polarization direction has been previously set such that an increase in voltage would preserve it. When the top electrode is the anode, the polarization points towards the cathode and the two charged sheets are positioned as in Figure 1. When the bottom electrode is used as the anode, the situation will be completely reversed but requires no special treatment from a theoretical point of view.

Solving the Poisson equation in each of the five regions of the ferroelectric is trivial with the current set of approximations and the solutions for the potential energy (W) and electric field (E) are given below:

Bottom electrode TL:

$$\begin{cases} W_b(x) = \dfrac{e\,N_d}{2\,\varepsilon_d^b\,\varepsilon_0}\,x^2 + A_b\,x + B_b \\ E_b(x) = \dfrac{e\,N_d}{\varepsilon_d^b\,\varepsilon_0}\,x + A_b. \end{cases} \tag{1}$$

Bottom electrode IL:

$$\begin{cases} W_p(x) = \dfrac{q_b}{2\,\varepsilon\,\varepsilon_0}\,x^2 + A_p\,x + B_p \\ E_p(x) = \dfrac{q_b}{\varepsilon\,\varepsilon_0}\,x + A_p, \end{cases} \tag{2}$$

the index p refers to the fact that the IL is formed in the vicinity of the positively charged sheet and q_b is the charge density in the IL.

For the top electrode IL:

$$\begin{cases} W_n(x) = \dfrac{q_t}{2\,\varepsilon\,\varepsilon_0}\,x^2 + A_n\,x + B_n \\ E_n(x) = \dfrac{q_t}{\varepsilon\,\varepsilon_0}\,x + A_n, \end{cases} \tag{3}$$

the index n refers to the fact that the IL is formed in the vicinity of the negatively charged sheet and q_t is the charge density in the IL.

Lastly, for the top electrode TL:

$$\begin{cases} W_t(x) = \dfrac{e\,N_d}{2\,\varepsilon_d^t\,\varepsilon_0}\,x^2 + A_t\,x + B_t \\ E_t(x) = \dfrac{e\,N_d}{\varepsilon_d^t\,\varepsilon_0}\,x + A_t, \end{cases} \tag{4}$$

where, A_b, B_b, A_p, B_p, A_n, B_n, A_t and B_t are integration constants that will be obtained from the continuity and boundary conditions and ε_d^b, ε_d^t and ε are the dielectric constants in the TLs and the ferroelectric bulk, respectively. It should be noted that according to the assumptions detailed above, the potential energy in the bulk region W_{bulk} is position-independent and the electric field is zero.

The boundary conditions should be satisfied by the potential energy at the two interfaces while the continuity conditions and the Gauss theorem will be used at the two charge sheets and in the ILs to obtain all the integration constants in equations (1)−(4):

Boundary conditions:

$$\begin{cases} W_b(0) = \Phi_b \\ W_t(d) = \Phi_t - V_a, \end{cases} \tag{5}$$

where Φ_b and Φ_t are the potential energy offsets at the two interfaces and V_a is the applied voltage on the top electrode.

Potential energy continuity conditions:

$$\begin{cases} W_b(d_b) = W_p(d_b) \\ W_n(d-d_t) = W_t(d-d_t) \\ W_p(d_b+w_b) = W_{bulk} = W_n(d-d_t-w_t), \end{cases} \tag{6}$$

where d_b, d_t, w_b and w_t are the widths of the TLs and ILs at the bottom and top electrodes, respectively and will be used as fitting parameters.

Electric field continuity conditions:

$$\begin{cases} E_p(d_b+w_b) = 0 \\ E_n(d-d_t-w_t) = 0. \end{cases} \tag{7}$$

Electric displacement jump at each charge sheet:

$$\begin{cases} \varepsilon\,\varepsilon_0\,E_p(d_b) - \varepsilon_d^b\,\varepsilon_0\,E_b(d_b) & = +P \\ \varepsilon_d^t\,\varepsilon_0\,E_t(d-d_t) - \varepsilon\,\varepsilon_0\,E_n(d-d_t) & = -P. \end{cases} \tag{8}$$

By solving the system of equations all the integration constants can be computed. The value of the potential energy in the bulk region, W_{bulk}, can be obtained by following an

approach developed by Nilsson [33] where the Fermi distribution of electrons in a bulk semiconductor with a dopant density N_d can be inverted with the following approximate formula:

$$\frac{W_{bulk}}{k_B\,T} = \frac{\mu_0}{k_B\,T} - \left[\frac{\ln r}{1-r} + \left(\frac{3\sqrt{\pi}}{4}r\right)^{\frac{2}{3}} + \frac{8\sqrt{\pi}}{3\,(4+r\sqrt{\pi})^2}r\right], \tag{9}$$

where $r = \frac{N_d}{N_c}$, N_c is the effective density of states in the conduction band and μ_0 is the chemical potential in the bulk region.

Using equations (1)−(9) the potential energy profile can now be determined within the confines of the above set of approximations. At this point one should be able to calculate incoming and outgoing currents through both interfaces of the device. These can be generated by various mechanisms simultaneously: tunnelling, thermal, trap assisted etc. And should be accounted for as much as possible. Metal ferroelectric interfaces are usually studied from the perspective of the so called Schottky emission, which most of the time translates to thermionic emission with the addition of Schottky barrier lowering. Due to the fact that ferroelectric polarization induces large spatial variations of the potential energy at the extremities of the bulk region (as compared to the normal metal-ferroelectric band offsets), the present model will include the quantum tunnelling component of the current alongside the thermally generated one. Figure 1 shows the potential energy profile for the MFM device (the figure is not drawn to scale and the bulk region has been shortened in order to better illustrate the shape of the potential barriers at the two interfaces). The effect of the two polarization charge sheets strongly influences the width of the interface barriers and unlike a regular M/S interface the potential barrier at the cathode is considerably thinner than the potential barrier at the anode. Another major difference is obviously in the height of the anode barrier, where the polarization influence induces a much higher barrier than the initial metal-ferroelectric barrier offset. Moreover, when compared to the normal M/S interfaces, the Schottky effect on this internal barrier should make little to no difference. Therefore, the quantum tunnelling should play an important role in transiting the charge carriers through this area.

The computations proceed by splitting the currents through each interface into two categories: *incoming* currents from the metal electrodes into the ferroelectric and *outgoing* currents, from the ferroelectric into electrodes. Each category is assumed to be composed of a thermionic component and a quantum tunnelling one. In order to ensure that the charge neutrality is satisfied, a balance equation is imposed by asking that the total current through the device is conserved. The thermionic component of the incoming/outgoing current is calculated using the general Richardson formula [18]:

$$I_{therm}(V_a,\mu) = S_g\,\frac{e\,m\,k_B^2\,T^2}{2\,\pi^2\,\hbar^3}\,\exp\left(-\frac{W_{max}-\mu}{k_B\,T}\right),$$

where, m is the electron effective mass in the potential barrier region, S_g is the surface area of the device (usually this is taken as the surface area of the top electrode), T is the system temperature and W_{max} is the potential barrier maximum which will be different for the cathode and the anode (see Fig. 1). Lastly, μ is the chemical potential in the region where the thermionic current originates.

For the quantum tunnelling component of the current, the transmission coefficient must be calculated for each potential barrier and this can be achieved by using the Wentzel-Kramers-Brillouin (WKB) approximation. Therefore it is generally given by [34]:

$$D(E) = \exp\left[-\frac{2}{\hbar}\int_{x_2}^{x_1}\sqrt{2\,m\,(W(x)-E)}\;dx\right], \tag{10}$$

where, $W(x)$ is the profile of the potential energy barrier, and $x_{1,2}$ are the turning points of the potential energy at the energy level E, given by the equation $W(x_{1,2}) = E$. The tunnelling current can be further obtained by integrating the product of the supply function and the tunneling coefficient in equation (10) [35] over all energies in the relevant conduction band.

One important approximation used in our model is the hypothesis of a local thermodynamic equilibrium in the ferroelectric. This translates to an uniform local chemical potential in the ILs and bulk areas. This approximation, which can be motivated by the relatively small thickness of the film, obviously allows a semi-analytical approach of the computations. To obtain the relative position of the chemical potential, μ_0 in the bulk ferroelectric with respect to conduction band minimum, one may rely on the usual Fermi-Dirac statistics of a doped semiconductor [18] and make use of (9). This parameter is critical to calculating the total current, since it gives an indication about the existing population of electrons before the potential barrier at the anode. The chemical potential in the bulk ferroelectric can be obtained from the conservation of the total current through the device, using the following balance equation:

$$I^b_{in}(V,\mu_0) + I^t_{in}(V,\mu_0) = I^t_{out}(V,\mu_0) + I^b_{out}(V,\mu_0), \tag{11}$$

where, the *in* and *out* indexes refer to the sum of all the corresponding components of the currents.

Equation (11), although not analytically solvable, will result in the dependence of the chemical potential μ_0 on the applied voltage on the anode and with it the leakage current for the MFM capacitor can be calculated as:

$$I_{leak}(V) = I^t_{out}(V,\mu_0(V)) - I^t_{in}(V,\mu_0(V)). \tag{12}$$

3 Results and discussions

In order to investigate how the theoretical model presented in the previous section is able to fit real experimental data, measurements have been performed on three

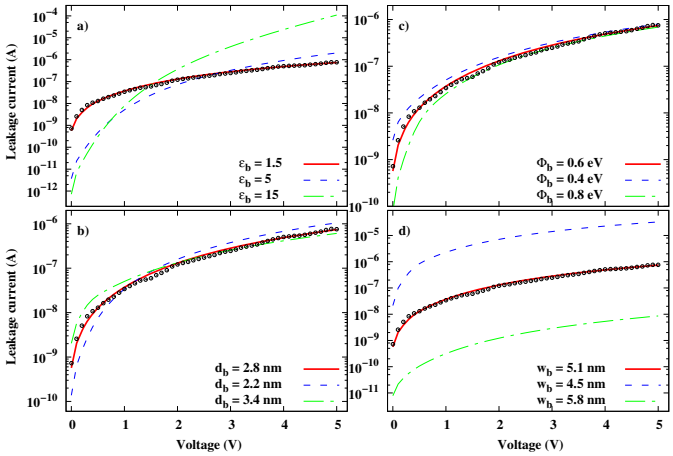

Fig. 2. Influence of the model parameters on the *I-V* curve and comparison with experimental data (hollow symbols). The values of each parameter for the bottom electrode were changed in turn from the best fit values (red continuous line) while maintaining the rest fixed. (a) TL dielectric permittivity; (b) interface potential barrier; (c) TL thickness; (d) IL width.

different MFM samples. They have been prepared with a common $SrRuO_3$ (SRO) bottom electrode (deposited on single crystal $SrTiO_3$) on top of which the ferroelectric $Pb(Zr_{0.2}Ti_{0.8})O_3$ (PZT) layer was epitaxially deposited by pulsed laser deposition with a thickness of 300 nm. Metallic top electrodes were later deposited on the PZT: SRO, Cu and Pt. The full details of the deposition process and the measurement technique are described elsewhere [16]. The *I-V* measurements were performed after the polarization state was set in the ferroelectric to point, in turn, towards the bottom and the top electrodes. This way it was possible to use both electrodes as the anode and investigate the possible role of the electrode on the *I-V* characteristics. Each sample was measured at three different temperatures ranging from 160 K to 310 K.

Equation (12) can be used to obtain the voltage dependence of the leakage current for the MFM capacitor with a number of parameters that need to be adjusted: the barrier heights at each interface (i.e. the conduction band offsets with respect to the electrodes, or interface potentials), TLs thicknesses, ILs widths and the dielectric permittivity for each TL. The experimental measurements were performed such that the polarization state was preserved. Thus, when the top electrode is the anode, the polarization points towards the bottom electrode and vice versa. Figure 2 illustrates the influence of the parameters related to the anode region (where the positive voltage is applied) on the *I-V* characteristics.

At this point it should be noted that all the fitting parameters were varied independently. This may obviously be considered as a limitation of the present model as compared, for example, to a more complex self-consistent treatment that would automatically incorporate the background relationships between various parameters. However, even with such inherent drawbacks, the present approach could still be used as a reasonably simple yet comprehensive way of investigating thin film MFM devices. The continuous line in each panel of Figure 2 represents the best fit curve for the experimental data shown in open symbols, while the dashed curves were obtained by deliberately modifying one of the four most important parameters at a time. As it can be seen, each of the four quantities contributes in a different way to the shape of the *I-V* curve. The dielectric permittivity of the TLs (Fig. 2a) seems to have the most important role in shaping the *I-V* in the high voltage region. The *I-V* characteristics measured for a variety of samples, display an interesting flattened shape in the high-voltage region, which would point to a dominance of the thermionic-type transmission of carriers in these voltage ranges. Nevertheless, the temperature dependence is not strong enough to suggest a thermionic type emission either. Instead, one must still consider an important contribution from the tunneling through the anode barrier, for which it turns out that a low value of the dielectric permittivity in the TLs ensures such a quasi-saturation of the emission current with the applied voltage. It can be assumed that, as an effect of the strong ferroelectric polarisation, both TL regions are flushed out of conduction electrons and their polarizability is inhibited by the strong local fields. The interface potential barrier (Fig. 2b) only has a marginal effect at low voltages. This is due to the fact that the offset between the electrode work function and the ferroelectric affinity, pales in comparison to the overall potential barrier height created by the ferroelectric polarization in the anode region (see Fig. 1). The TL thickness (Fig. 2c) has an almost similar influence as the interface potential barrier since, over a certain value of the applied voltage, there are no significant changes to the main anode barrier height or thickness, the electron emission being controlled almost entirely by the value of the dielectric constant in the TL. The parameter that changes the overall value of the emission current is the IL thickness (Fig. 2d). Since the electrons will occupy states with energies in the vicinity of the conduction band minimum, this is where the emission will most likely take place from. The IL thickness controls the biggest part of the potential barrier thickness as it is "seen" by an incoming electron. Moreover, the IL is directly influenced by the ferroelectric polarization and will not depend strongly on temperature or on the top electrode. This behaviour is in direct contrast with the general theory for the metal/semiconductor contacts where the depletion width has a strong voltage dependence.

Figure 3 shows the experimental *I-V* characteristics for three samples with different top electrodes (SRO in Fig. 3a, Cu in Fig. 3b and Pt in Fig. 3c) that were fitted with the current theoretical model. The experimental data have been collected at three different temperatures above 150 K and each characteristic has been taken by exchanging the role of the anode between the two electrodes (the anode electrode is indicated on the corresponding branches of the diagrams). The average values of the fitting parameters are detailed in Table 1. These values were obtained by considering first the bottom electrode, then

Table 1. Average values for the parameters used in the fitting of the experimental data of Figure 3.

Bottom electrode				Top electrode			
ε_d^b	d_b (nm)	w_b (nm)	Φ_b (eV)	ε_d^t	d_t (nm)	w_t (nm)	Φ_t (eV)
SRO				SRO			
5.93	4	5.08	0.5	2.4	3.23	5.32	0.8
SRO				Cu			
2.23	3.2	4.94	0.5	2.2	4	4.85	0.7
SRO				Pt			
8.23	3.8	5.12	0.5	2.16	1.96	5.3	1

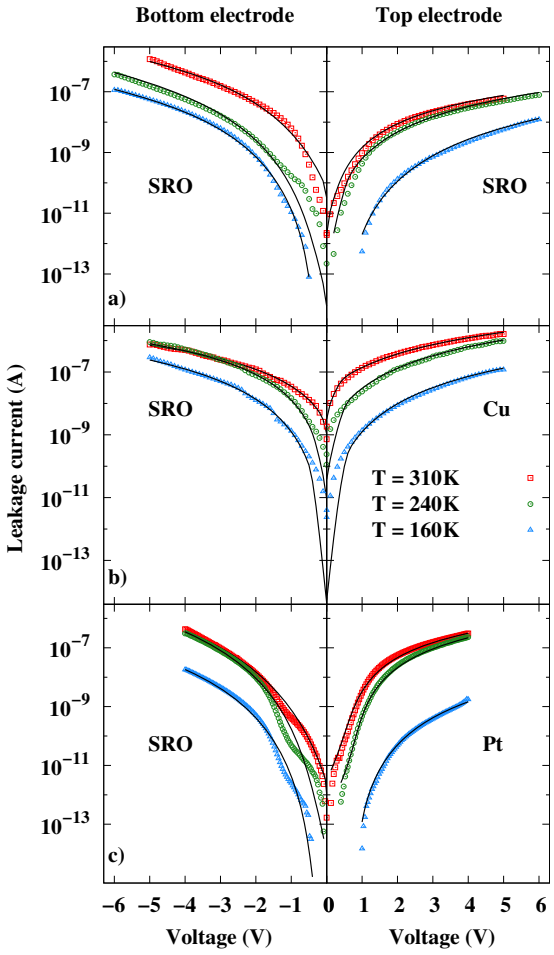

Fig. 3. Best fit curves (continuous black lines) for three top electrode materials and three system temperatures shown in open symbols.

the top one as the anode. The rest of the parameters used in this model were considered constant and assigned reasonable values from the literature: $N_d = 4.5 \times 10^{25}$ m^{-3}, $\varepsilon = 200$ and $P = 0.9$ C m^{-2} [10,12,14–17,36].

The values obtained in Table 1 are very consistent and one indication for this consistency is in the values for the IL thickness: since all samples have the same epitaxial ferroelectric layer, one would expect that the polarization will have the same impact on the charge distribution, such that similar values would result for the cathode and the anode IL thickness. The small differences that can be observed between samples can be the result of small variations in the value of the ferroelectric polarization or a decrease in the degree of epitaxy at the top-electrode interface. The consistency of the model is also given by the values obtained for the interface potential barriers at each interface. The bottom electrode interface has the same value for each sample since this is the common interface, while the barrier height at the top electrode interface is different, depending on the used material. One interesting fact can be noted for the SRO top electrode, where the potential barrier height was different than that for the bottom electrode. This may be due to the decrease in the degree of epitaxy over the thickness of the ferroelectric, which makes the top electrode interface not exactly identical to the bottom one, thus resulting in a different set of parameters. One should note however that there are some discrepancies between the barrier heights obtained with this model and the ones presented in reference [16]. The reason lies in the fact that a single-interface model with a Schottky electron transfer mechanism was used in that case, and the results were expected to differ from the ones presented in this work where the problem is analysed from an integrated, two-interface point of view.

While both interface barriers and the IL widths are weakly coupled with the applied voltage, the remaining parameters, dielectric permittivity and thickness of the TLs, can be used to better differentiate between the three samples. It appears that, depending on the material used as top electrode, the interface regions are affected simultaneously in different manners. First, the dielectric permittivity of each TL is much lower than the value considered in the rest of the ferroelectric, $\varepsilon = 200$. Moreover, although all three samples have a common SRO interface, the values of ε_d^b are affected by the top electrode, contributing to the argument that the ferroelectric together with both its interfaces should be considered as a whole system. Also, with the exception of *Cu*, $\varepsilon_d^t < \varepsilon_d^b$, suggesting that the top electrode interface has a much stronger effect on the polarizability of the neighbouring TL. The behaviour observed for the dielectric permittivity of the TL is in good agreement with the calculations performed by Stengel and Spaldin in reference [24]. They have noted that, what they call "intrinsic dead layer", is a transition zone between an ideal insulator and a metal where the polarizability falls dramatically with respect to the bulk ferroelectric material. This result is shown in Figure 4 where the inverse dielectric permittivity is represented as a function of position and each zone is shaded in the same fashion as in Figure 1.

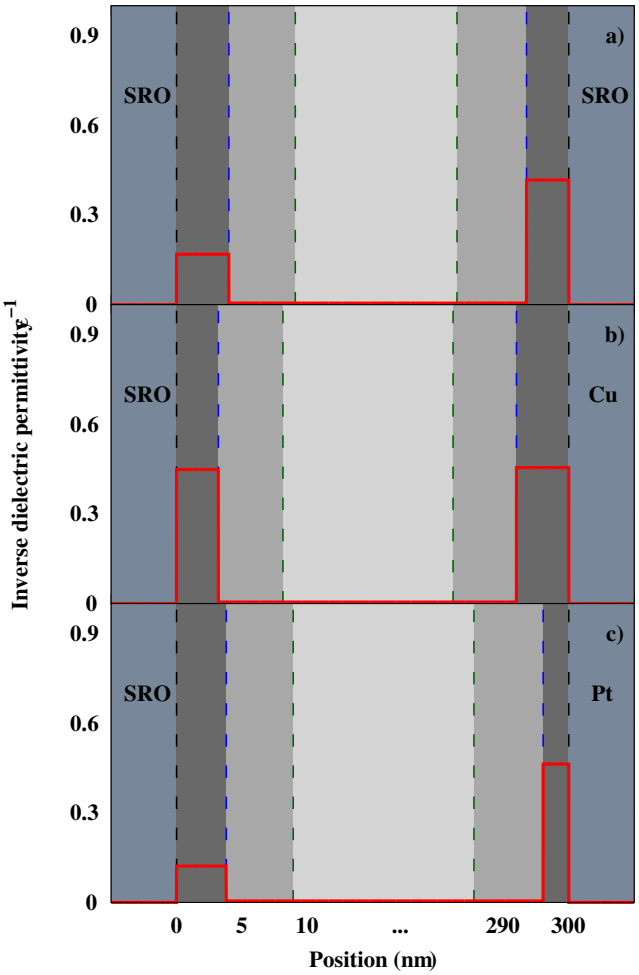

Fig. 4. Inverse dielectric permittivity as a function of position for the entire MFM structure for each of the three electrode combinations: (a) SRO/PZT/SRO; (b) SRO/PZT/Cu; (c) SRO/PZT/Pt. The shaded sections follow the same scheme as in Figure 1.

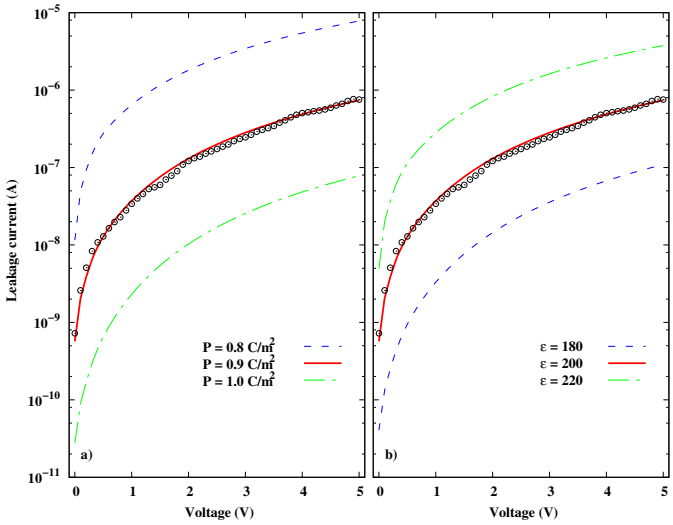

Fig. 5. Influence of the polarization (a) and the dielectric constant of the ferroelectric bulk value (b) on the I-V characteristics and comparison with experimental data (hollow symbols). The P and ε values were changed from the best fit values (red continuous line) while maintaining the rest of the parameters fixed.

The two peaks in each of the three cases, represent the TL regions for each interface. In this view, it becomes evident that, depending on the material chosen for the top electrode and the growth conditions, the MFM system will have a different behaviour. Even if ε_d^i may not be strictly identified as dielectric constants of the TLs (due to the various model simplifications, especially the very schematic spatial distribution of the polarisation), the trend observed by Stengel and Spaldin [24] can still be considered as confirmed through this completely independent approach.

A final point must be discussed about the values obtained for the fitting parameters in Table 1. They are clearly dependent on two specified quantities, namely the saturated polarization P and the dielectric constant in the ferroelectric bulk, ε. It must be stressed out that, while their values in our computations are suggested in the current literature, they have both quite large margins of uncertainty. For example, the determination of the dielectric permittivity in the bulk area of the film is always contaminated by the different polarizability of the transition layers [24] in the areas of the electrode interfaces. Moreover, both quantities may show variations with temperature, which, for reasons of insufficient reliable data, we have disregarded in our fitting procedures. It would be therefore of interest to investigate how the variation of the ferroelectric polarization, P or the dielectric constant ferroelectric bulk, ε may affect the computed I-V characteristics. This analysis is summarized in Figure 5.

It may be seen that any decrease in P (Fig. 5a) or an increase of ε (Fig. 5b), would translate the diagrams towards higher currents. This trend can be easily compensated by increasing the $w_{b,t}$ value, which would pull the diagram downwards as it is shown to happen in Figure 2d. Therefore, any imprecision in P or ε would translate in the uncertainty of the extent of the corresponding IL and any temperature variations of these two quantities would imply a corresponding variation of $w_{b,t}$. For example, it is known that the dielectric constant increases when the sample is heated from low temperatures towards the room ambient ones. This determines a corresponding shift towards higher values of the I-V diagrams, which should be compensated by an increase of the fitting values for $w_{b,t}$ with temperature, which is clearly physically plausible. The same effect would also have the expected decrease of the polarization values, P with temperature. The current theoretical model has been used to successfully fit experimental data for various structural and thermal conditions. However there are still a number of parameters which should be obtained experimentally with higher degree of accuracy before a quantitative analysis can be performed. Nevertheless, this model can be used to investigate trends for the variation of the involved parameters of a thin film MFM system under different conditions.

4 Conclusions

The present theoretical model outlines the importance of considering together the two interfaces of the thin film MFM device. Even if very schematic, the approach is able to accurately reproduce and to some extent predict, how parameters such as the potential barrier heights, dielectric constants, influence and transition layer widths can act on the leakage current. The results of the model related to spatial variation of the dielectric constant in the ferroelectric are also in good agreement with independent numerical calculations performed on similar structures. However, it should be noted that this treatment is strongly simplified in that the ferroelectric polarization is considered via the abrupt approximation, as produced by a pair of charged sheets. In reality, it is expected that the polarization gradually decreases in the TL regions towards zero at the electrode interface. Such an approach would need a much more complex treatment of the entire system, in a self-consistent procedure, of which the present model can be considered as a first approximation.

Author contribution statement

All authors contributed equally.

Author Lucian D. Filip would like to acknowledge the financial support of the Romanian Ministry of Education-Executive Unit for Funding High Education, Research, Development and Innovation (MEN-UEFISCDI) through the Young Research Team Grant PNII-RU-TE-2012-3-0320 (Contract No. 11). Author Lucian Pintilie would like to acknowledge the financial support of the Romanian Ministry of Education-Executive Unit for Funding High Education, Research, Development and Innovation (MEN-UEFISCDI) through the Idea-Complex Research Grant PN-II-ID-PCCE-2011-2-0006 (contract No. 3/2012).

References

1. C.A. Mead, Phys. Rev. Lett. **6**, 545 (1961)
2. C. Zhou, D.M. Newns, J. Appl. Phys. **82**, 3081 (1997)
3. J.F. Scott, Annu. Rev. Mater. Sci. **28**, 79 (1998)
4. B. Nagaraj, S. Aggarwal, T.K. Song, T. Sawhney, R. Ramesh, Phys. Rev. B **59**, 16022 (1999)
5. B. Nagaraj et al., Appl. Phys. Lett. **74**, 3194 (1999)
6. B. Nagaraj, S. Aggarwal, R. Ramesh, J. Appl. Phys. **90**, 375 (2001)
7. C.T. Black, J. Welser, Electron Devices IEEE Trans. **46**, 776 (1999)
8. J.F. Scott, *Ferroelectric Memories* (Springer, Berlin, New York, 2000)
9. L.J. Sinnamon, R.M. Bowman, J.M. Gregg, Appl. Phys. Lett. **78**, 1724 (2001)
10. T.P. Juan, S. Chen, J.Y.m. Lee, J. Appl. Phys. **95**, 3120 (2004)
11. J.D. Baniecki, T. Shioga, K. Kurihara, N. Kamehara, J. Appl. Phys. **97**, 114101 (2005)
12. P. Zubko, D.J. Jung, J.F. Scott, J. Appl. Phys. **100**, 114112 (2006)
13. M.T. Chentir, E. Bouyssou, L. Ventura, C. Anceau, J. Appl. Phys. **105**, 061605 (2009)
14. L. Pintilie, I. Vrejoiu, D. Hesse, G. LeRhun, M. Alexe, Phys. Rev. B **75**, 104103 (2007)
15. L. Pintilie, V. Stancu, L. Trupina, I. Pintilie, Phys. Rev. B **82**, 085319 (2010)
16. I. Pintilie, C.M. Teodorescu, C. Ghica, C. Chirila, A.G. Boni, L. Hrib, I. Pasuk, R. Negrea, N. Apostol, L. Pintilie, ACS Appl. Mater. Interfaces **6**, 2929 (2014)
17. P. Juan, H. Chou, J. Lee, Microelectron. Reliab. **45**, 1003 (2005)
18. S.M. Sze, *Physics of Semiconductor Devices* (Wiley, New York, 1981)
19. R. Kretschmer, K. Binder, Phys. Rev. B **20**, 1065 (1979)
20. M. Hideharu, New J. Phys. **2**, 8 (2000)
21. J. McAneney, L.J. Sinnamon, R.M. Bowman, J.M. Gregg, J. Appl. Phys. **94**, 4566 (2003)
22. O.G. Vendik, S.P. Zubko, N.Y. Medvedeva, J. Appl. Phys. **105**, 053515 (2009)
23. V.M. Voora, T. Hofmann, M. Brandt, M. Lorenz, M. Grundmann, N. Ashkenov, H. Schmidt, N. Ianno, M. Schubert, Phys. Rev. B **81**, 195307 (2010)
24. M. Stengel, N.A. Spaldin, Nature **443**, 679 (2006)
25. L.W. Chang, M. Alexe, J.F. Scott, J.M. Gregg, Adv. Mater. **21**, 4911 (2009)
26. H. Schroeder, S. Schmitz, Appl. Phys. Lett. **83**, 4381 (2003)
27. Y. Wang, M.K. Niranjan, K. Janicka, J.P. Velev, M.Y. Zhuravlev, S.S. Jaswal, E.Y. Tsymbal, Phys. Rev. B **82**, 094114 (2010)
28. B. Chen, H. Yang, J. Miao, L. Zhao, L.X. Cao, B. Xu, X.G. Qiu, B.R. Zhao, J. Appl. Phys. **97**, 024106 (2005)
29. M.S. Majdoub, R. Maranganti, P. Sharma, Phys. Rev. B **79**, 115412 (2009)
30. C. Ge, K.J. Jin, C. Wang, H.B. Lu, C. Wang, G.Z. Yang, J. Appl. Phys. **111**, 054104 (2012)
31. C. Ge, K.J. Jin, C. Wang, H.B. Lu, C. Wang, G.Z. Yang, Appl. Phys. Lett. **99**, 063509 (2011)
32. M. Dawber, J.F. Scott, J. Phys.: Condens. Matter **16**, L515 (2004)
33. N.G. Nilsson, Phys. Stat. Sol. A **19**, K75 (1973)
34. B.H. Bransden, C.J. Joachain, *Quantum Mechanics* (Prentice Hall, Harlow, New York, 2000)
35. E.L. Murphy, R.H. Good, Phys. Rev. **102**, 1464 (1956)
36. C.S. Hwang, B.T. Lee, C.S. Kang, K.H. Lee, H.J. Cho, H. Hideki, W.D. Kim, S.I. Lee, M.Y. Lee, J. Appl. Phys. **85**, 287 (1999)